FDG PET, which has been used extensively to differentiate post-treatment change and viable tumor in the brain (*13,14*), has not been routinely applied to image neoplastic involvement of the spinal cord. Evaluation of the spinal cord with PET is, in part, limited by scanner spatial resolution, with compromised sensitivity for the detection of hypermetabolic lesions smaller in size than approximately 2.5 times the scanner spatial resolution (*15,16*). However, current whole-body PET scanners with resolutions of 4–6 mm FWHM are well suited to extending imaging of CNS tumors below the neck.

Since the normal spinal cord is comprised of a relatively large amount of axonal white matter, it manifests lower FDG uptake than cortical brain tissue on PET imaging. The glucose metabolic rate of white matter is approximately one-third to one-fourth that of white matter (*17*); therefore, tumor-to-background contrast should be more favorable in the spinal cord than in cortical brain regions. This has been verified by Di Chiro et al. (*11*), who reported a glucose metabolic rate of 1.7 mg/100 gm brain tissue/min for normal spinal cord (compared to values of 6.0–7.0 for midbrain pons area) using a tomograph. Holtoff et al. (*9*) reported glucose metabolic rates that were mildly lower than those of cerebral gray matter in two cases of PNET. Tumor-to-white matter ratios in these two cases were approximately 1.9 and 1.1. Interestingly, this group reported glucose metabolic rates of nearly twice that of PNET in the histologically similar medulloblastoma. In accord with the findings of Holtoff et al. (*9*), the spinal cord PNET lesion in our case was hypermetabolic relative to the unaffected spinal cord but similar in FDG uptake to the cerebellum. Prior radiation therapy to the entire neural axis may have diffusely lowered baseline FDG uptake in all nontumor CNS tissue, further contributing to increased lesion-to-spinal cord contrast.

CONCLUSION

The most clinically useful role of FDG PET imaging in patients with CNS neoplasms has been in the diagnosis of suspected tumor recurrence. In this setting, CT or MRI may be indeterminant due to anatomical distortion from surgical-, radiation- and/or chemotherapy-induced changes (*18*). PET has been effectively used to noninvasively distinguish active tumor from post-treatment effects in the brain. This case report illustrates that, with the recent progress in PET technology, it is now feasible to use FDG PET in the evaluation of spinal cord neoplasms.

REFERENCES

1. Ishikawa M, Kikuchi H, Miyatake S, Oda Y, Yonekura Y, Nichizawa S. Glucose consumption in recurrent gliomas. *Neurosurgery* 1993;33:28–33.
2. Patronas NJ, Di Chiro G, Kufta C, et al. Prediction of survival in glioma patients by means of positron emission tomography. *J Neurosurg* 1985;62:816–822.
3. Alavi JB, Alavi A, Chawluk J, et al. Positron emission tomography in patients with glioma. A predictor of prognosis. *Cancer* 1988;62:1074–1078.
4. Hoffman JM, Lowe VJ, Brown M, Burger P, Hanson MW, Coleman RE. The prognostic and diagnostic usefulness of FDG-PET in primary brain tumor management [Abstract]. *J Nucl Med* 1993;34:37P.
5. Mineura K, Sasajima T, Kowada M, et al. Perfusion and metabolism in predicting the survival of patients with cerebral gliomas. *Cancer* 1994;73:2386–2394.
6. Rosenfeld SS, Hoffman JM, Coleman RE, Glantz MJ, Hanson MW, Schold SC. Studies of primary central nervous system lymphoma with fluorine-18-fluorodeoxyglucose positron emission tomography. *J Nucl Med* 1992;33:532–536.
7. Kuwabara Y, Ichiya Y, Otsuka M, et al. High ^{18}F-FDG uptake in primary cerebral lymphoma: a PET study. *J Comput Assist Tomogr* 1988;12:47–48.
8. Di Chiro G, Hatazawa J, Katz DA, Rizzoli HV, De Michele DJ. Glucose utilization by intracranial meningiomas as an index of tumor aggressivity and probability of recurrence: a PET study. *Radiology* 1987;164:521–526.
9. Holthoff VA, Herholz K, Berthold F, et al. In vivo metabolism of childhood posterior fossa tumors and primitive neuroectodermal tumors before and after treatment. *Cancer* 1993;72:1394–403.
10. Griffeth LK, Rich KM, Dehdashti F, et al. Brain metastases from non-central nervous system tumors: evaluation with PET. *Radiology* 1993;186:37–44.
11. Di Chiro G, Oldfield E, Bairamian D, et al. Metabolic imaging of the brain stem and spinal cord: studies with positron emission tomography using ^{18}F-2-deoxyglucose in normal and pathological cases. *J Comput Assist Tomogr* 1983;7:937–945.
12. Sasajima T, Mineura K, Itoh Y, et al. Spinal cord ependymoma: a positron emission tomographic study with (^{11}C-methyl)-L-methionine. *Neuroradiology* 1996;38:53–55.
13. Doyle WK, Budinger TF, Valk PE, Levin VA, Gutin PH. Differentiation of cerebral radiation necrosis from tumor recurrence by ^{18}F-FDG and ^{82}Rb positron emission tomography. *J Comput Assist Tomogr* 1987;11:563–570.
14. Glantz MJ, Hoffman JM, Coleman RE, et al. Identification of early recurrence of primary central nervous system tumors by ^{18}F-fluorodeoxyglucose positron emission tomography. *Ann Neurol* 1991;29:347–355.
15. Hoffman EJ, Huang SC, Phelps ME. Quantitation in positron emission CT: 1. Effect of object size. *J Comput Assist Tomogr* 1979;3:299–308.
16. Kessler RM, Ellis JR, Eden M. Analysis of emission tomographic scan data: limitations imposed by resolution and background. *J Comput Assist Tomogr* 1984;8: 514–522.
17. Mazziotta JC, Phelps ME, Plummer D, Kuhl DE. Quantitation in positron emission tomography: 5. Physical-anatomical effects. *J Comput Assist Tomogr* 1981;5:734–743.
18. Dooms GC, Hecht S, Brant-Zawadski M, Berthiaume Y, Norman D, Newton TH. Brain radiation lesions: MR imaging. *Radiology* 1986;158:149–155.

Investigation of Angiotensin II/AT$_1$ Receptors with Carbon-11-L-159,884: A Selective AT$_1$ Antagonist

Zsolt Szabo, Pan Fu Kao, H. Donald Burns, Raymond E. Gibson, Terence G. Hamill, Hayden T. Ravert, Sang Eun Kim, William B. Mathews, John L. Musachio, Ursula Scheffel and Robert F. Dannals

Division of Nuclear Medicine, The Johns Hopkins Medical Institutions, Baltimore, Maryland; and Department of Pharmacology, Merck Research Laboratories, West Point, Pennsylvania

Antagonists of the angiotensin II AT$_1$ receptor subtype have been recently introduced for treatment of arterial hypertension and for pharmacological studies of these receptors. The purpose of this work was to label such an antagonist with ^{11}C and test the applicability of the radioligand for PET studies. **Methods:** The potent and selective nonpeptide AT$_1$ antagonist L-159,884 was labeled with ^{11}C and injected intravenously into six dogs. Renal accumulation and kinetics of the radioligand were imaged with PET at baseline and after receptor blockade with 1 mg/kg MK-996. Time-activity curves were derived from the renal cortex and were analyzed by the Gjedde-Patlak plot to obtain the influx rate constant of the radioligand. **Results:** There was selective radioligand binding in the kidneys, mainly located in the cortex. Within the time interval between 95 and 115 min postinjection, the radioactivity retained in the kidneys was 109 ± 27 and 42 ± 4 nCi/ml/mCi of the injected dose for the control and inhibition studies, respectively. The influx rate constant of the radioligand decreased from a baseline of 0.0298 ± 0.0156 to a post-MK-996 value of 0.0098 ± 0.0052. **Conclusion:** These results demonstrate distinct binding of ^{11}C-L-159,884 in the renal cortex with a specific binding component suitable for quantitative PET imaging of angiotensin II/AT1 receptors.

Key Words: PET; kidney; carbon-11; substituted benzoyl sulfonamides; dogs; angiotensin receptors

J Nucl Med 1998; 39:1209–1213

Received Jan. 16, 1997; revision accepted Oct. 13, 1997.

For correspondence or reprints contact: Zsolt Szabo, MD, PhD, Division of Nuclear Medicine, The Johns Hopkins Medical Institutions, Nelson Building B1-119, 600 North Wolfe St., Baltimore, MD 21030.

The AT_1 angiotensin II (Ang II) receptor mediates all known physiological effects of Ang II, including regulation of arterial blood pressure, heart rate, aldosterone secretion, renal blood flow, glomerular filtration, and sodium and water reabsorption (*1–3*). The renin-angiotensin system, largely by way of the AT_1 receptors, is also implicated in renovascular disease and other forms of arterial hypertension (*4–7*).

Despite the importance of the AT_1 receptor subtype, there is no direct technique available for its in vivo investigation. At present, these receptors can only be quantitated ex vivo in animals or postmortem in human tissues. This article reports details of PET studies of AT_1 receptors using a ^{11}C-labeled substituted benzoyl sulfonamide, a nonpeptide AT_1-selective Ang II receptor antagonist.

Substituted benzoyl sulfonamides appear more suitable for PET than the clinically used nonpeptide AT_1 antagonist, losartan; they are more potent, and unlike losartan, they do not require metabolic conversion to bind with subnanomolar affinity to AT_1 receptors (*8*). The drug MK-996 is a potent nonpeptide AT_1-selective antagonist (*9*) that has been shown to improve arterial blood pressure in patients with mild-to-moderate essential hypertension (*10*). In this study, a ^{11}C-labeled methoxy-substituted analog of MK-996, *N*-[[4′-[(2-ethyl-5,7-dimethyl-^{3}H-imidazo[4,5-B]pyridin-3-yl)methyl][1,1′-biphenyl]−2-yl]sulfonyl]-4-methoxybenzamide (L-159,884), was injected intravenously into dogs, and its accumulation and kinetics in the kidneys were studied. The kidneys were selected for imaging because of the abundance and physiological significance of AT_1 receptors in this organ.

The time-activity curves derived from the renal cortex were analyzed by the Gjedde-Patlak plot. From this graph, the influx rate constant was derived, and the effect of the receptor antagonist MK-996 on radioligand binding was quantified.

MATERIALS AND METHODS

Radiotracer Synthesis

The normethyl precursor L-162,914, obtained from Merck Research Laboratories (Rahway, NJ), was labeled by ^{11}C methylation (*11*). The resulting ^{11}C-L-159,884 was isolated by reverse phase high-performance liquid chromatography (HPLC). The average synthesis time was 18 min from the end of bombardment, and the nondecay-corrected radiochemical yield was 5% at an average specific activity of 2980 mCi/μmol. [See Hamill et al. (*12*) for a more detailed description of this synthesis.]

Animal Preparation

The experimental protocol was approved by the Animal Care and Use Committee of the Johns Hopkins Medical Institutions. Six beagle dogs, weighing 7.7–14.6 kg (11.0 ± 2.3 kg), were used for the experiments. The animals fasted for at least 12 hr, given water ad libitum and premedicated with 0.3–0.4 ml of acepromazine injected intramuscularly on the day of the experiment. A 20-gauge 2-in. venous catheter was placed into the right frontal leg ulnar vein, through which anesthesia was introduced by injection of sodium pentobarbital (25–30 mg/kg) and was maintained later with additional pentobarbital at an average dose of 3 mg/kg/hr. Another catheter was inserted into the contralateral ulnar vein for radiotracer administration.

Oxygen saturation of circulating blood was measured with a pulse oximeter (Nellcor, Hayward, CA) placed on the tongue of the animal. Circulatory volume was maintained by intravenous infusion of isotonic saline. A 22-gauge cannula was inserted in the anterior tibial or distal femoral artery for continuous pressure monitoring (Model 90603A, Spacelabs, Medical, Inc., Redmond, WA). Electrocardiogram, heart rate and core temperature were monitored continuously. In particular, the electrocardiogram was observed for ST segment changes and arrhythmias.

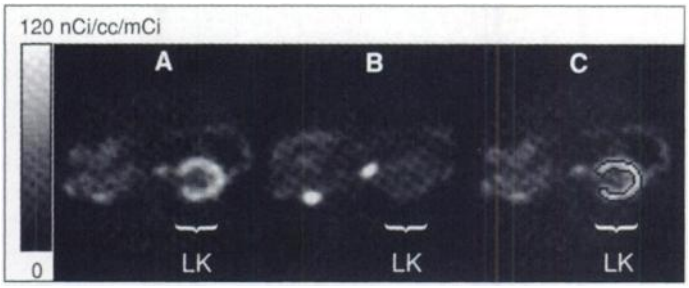

FIGURE 1. Images of midabdominal area of dog obtained 55–115 min postinjection ^{11}C-L-159,884. (A) Control study. (B) Study after pretreatment with 1 mg/kg MK-996. (C) Region of interest used to derive time-activity curves from renal cortex. Hot spots outside area of kidney are due to tracer accumulation in small bowel. LK = left kidney.

PET Imaging

PET studies were performed with a GE 4096+ (GE Medical Systems, Milwaukee, WI) PET scanner with an average in-plane–cross-plane spatial resolution of FWHM = 6 mm. The animals were positioned with both kidneys included in the field of view of the PET scanner. A transmission scan with a 10-mCi ^{68}Ge pin source was obtained first and was used subsequently for attenuation correction of the PET scans. In each animal, two experiments were performed, with an interval of 3 hr between the two tracer injections. At baseline, the dogs received 17 ± 4 mCi of ^{11}C-L-159,884 injected intravenously as a slow (15-sec) bolus with a specific activity of 1391 ± 563 mCi/μmol. Thirty minutes after conclusion of PET imaging, MK-996 (1 mg/kg) was injected intravenously slowly (over a 5-min interval). Thirty minutes postadministration of the MK-996 blocking dose, a second tracer dose (13 ± 7 mCi; specific activity = 1344 ± 588 mCi/μmol) was administered, and PET imaging was started again.

Dynamic PET studies were acquired with the following image sequence: four images of 15-sec duration, three images of 1-min duration, three images of 2-min duration, three images of 5-min duration, three images of 10-min duration and three images of 20-min duration, with a total imaging time of 115 min. The PET images were reconstructed by filtered backprojection of the sinograms using a ramp filter only. For display purposes (Fig. 1), the images were convolved with a 3 × 3 pixel smoothing kernel.

After attenuation correction and decay correction, the PET images were transferred via ethernet to a personal computer supplied with an Intel Pentium Pro 200-MHz (Intel Corp., Santa Clara, CA) processor. Using the Johns Hopkins University program "Imager," regions of interest were defined over the cortex of both kidneys (Fig. 1C). An average of the left and right renal cortical activities was used for data analysis. Time-activity curves, expressed in nanocuries per milliliters per millicuries of the injected dose, were further processed using Microsoft Excel/Windows 95 (Microsoft Corp., Redmond, WA) and Matlab/Windows 95 (The Math Works Inc., Natick, MA).

Arterial Input Function

Total plasma radioactivity was measured in blood samples collected from a femoral artery as quickly as possible during the first 2 min (every 3–10 sec) and at increasing time intervals thereafter. The plasma activity was corrected for physical decay and expressed as nanocuries per cubic centimeter per millicurie of the injected dose. At distinct time points (5, 15, 30 and 60 min postinjection), an additional 2 ml of arterial blood were collected for determination of metabolites. After centrifugation, 1 ml of plasma was separated and placed in a test tube. One milliliter of 5% perchloric acid in the high-performance liquid chromatography

(HPLC) mobile phase was added to precipitate plasma proteins, mixed thoroughly and centrifuged for 10 min at 2000 rpm. One milliliter of supernatant was taken and injected onto HPLC with a Waters pump (Waters Associates, Milford, MA), an Alltech Econosil C_{18} column (Alltech Associates, Deerfield, IL) and a radioactivity detector connected to an online computer for data acquisition and processing. The HPLC mobile phase consisted of 20% acetonitrile, 40% methanol and 40% H_2O with 0.1% trifluoroacetic acid. The retention time of the metabolites was 2 to 3 min, and the retention time of ^{11}C-L-159,884 was 5–6 min.

Data Processing

Because radioligand metabolites were measured only at limited time points, additional time points were calculated by monoexponential interpolation/extrapolation to obtain the sampling rate needed for curve processing.

To assess the effect of the AT_1 receptor antagonist MK-996 on total and metabolite-corrected plasma radioactivity, these time–activity curves were displayed in both a linear and a semilogarithmic fashion and were compared by numerical integration:

$$\int_{t_0=0}^{t_n=T} C_p(t)dt = \frac{\sum_{i=1}^{n}\left[C_p(i) + C_p(i-1)\right][t_i - t_{i-1}]}{2}, \quad \text{Eq. 1}$$

where $C_p(t)$ is the continuous representation, and $C_p(i)$ is the discrete representation of plasma radioactivity.

From the tissue activity curve region, plasma activity curve and the plasma activity time-integral a Gjedde–Patlak plot was created (*13–15*):

$$\frac{ROI(T)}{C_p(T)} = V_0 + K_i\left(\frac{\int_{t=0}^{i=T} C_p(t)dt}{C_p(T)}\right). \quad \text{Eq. 2}$$

Parameter V_0 is the initial volume of distribution and the expression within the bracket of Equation 2 is called stretched time or normalized time (*16*). The normalized time is represented on the x-axis while the normalized tissue activity (the left side of Eq. 2) is represented on the y-axis. In the case of a radioligand with an irreversible kinetic component, the slope of this plot is equivalent to the influx rate constant K_i (*16*).

RESULTS

There was preferential accumulation of ^{11}C-L-159,884 in the renal cortex (Fig. 1A). The radioligand amount in the kidneys was significantly reduced by pretreatment with the AT_1 receptor antagonist MK-996 (Fig. 1B). A minimal amount of activity could also be observed in the collecting system, indicating minimal radioligand excretion (Fig. 1B).

As time elapsed after tracer administration, increasing radioactivity was observed in the liver, followed by accumulation in the gallbladder (image not shown) and, finally, in the loops of small bowel (Fig. 1A and B). Activity in the gastrointestinal system was separable from that in the kidneys, and placement of a region of interest delineating the renal cortex was unaffected (Fig. 1C).

The arterial input function increased to a peak value of over 2000 nCi/ml/mCi of the injected dose during the first 30 sec. This sharp increase was followed by a fast decline to <10% of the peak activity within 5 min. After a slower descent over a period of 5–40 min, total arterial radioactivity reached a constant value. Unmetabolized radioactivity decreased to a value of ~0.1% of the peak at 115 min postinjection (Fig.2A and B). Both total arterial and metabolite-corrected arterial activity were slightly higher after pretreatment with MK-996.

The time integral of total arterial activity was 8564 ± 1521 (range 6889–10,653) for the control studies and 11,287 ± 1615 (range 9953–13,831) after MK-996 treatment. The time integral of unmetabolized arterial activity was 3969 ± 2401 (range, 1638–7324) for the control studies and 5292 ± 2636 (range, 2557–8445) after MK-996 treatment.

The fraction of unmetabolized radioligand in arterial plasma was determined at four time points. Using these four data points, additional data points were reconstructed by monoexponential fitting (Fig. 2C). Unmetabolized radioligand decreased from 75% at 5 min to 25% at 60 min postinjection and was slightly less for the MK-996 group than for the control study (Fig. 2D), probably due to a higher amount of unbound circulating ligand available for metabolism.

Radioactivity in the cortices of the kidneys was highest during the first 30 sec and reached a value of 300 nCi/ml/mCi. After a faster decline with a half-life of ~15 min, radioactivity in the kidneys reached a constant value at around 60 min and remained almost constant until the end of the study (Fig. 3). The percentage difference between the control and MK-996 studies increased to ~50% at 60 min and remained stable until the end of the study (Fig. 3, inset).

The Gjedde-Patlak plot was linear for the last four points (Fig. 4), and using these four points, the slope was calculated to express the influx rate constant of the radioligand K_i. Parameter K_i decreased from a baseline of 0.0298 ± 0.0156 to a post-MK-996 value of 0.0098 ± 0.0052, indicating that specific binding of the radioligand comprised two-thirds of the total binding.

DISCUSSION

The presented PET images, time-activity curves and influx rate constants demonstrate binding of ^{11}C-L-159,884 at the site of the Ang II/AT_1 receptors in the renal cortex and encourage the application of this new radioligand for PET imaging studies.

Dogs were chosen for these preclinical studies because these animals represent a well-established model for investigations of the renin-angiotensin system, particularly the AT_1 receptors. In contrast to rats and mice, in which two subtypes, AT_{1a} and AT_{1b}, have been discovered, dogs, like humans, possess only one subtype of these receptors, e.g., AT_1 (*17*). An additional advantage of the dog model is that there is high degree of homology of the amino acid sequences between the dog and human AT_1 receptor proteins (*18*).

The drug MK-996 was chosen to assess nonspecific binding because it is a very potent antagonist of the AT_1 receptor. According to Kivlighn et al. (*19*), 0.1 mg/kg MK-996 produces peak inhibition of pressor responses to exogenous Ang II as early as 5 min after intravenous injection in conscious normotensive dogs. Peak inhibition plateaus and is maintained for 90 min, followed by a steady decrease with a 50% effect remaining 4 hr postinjection. An intravenous dose of 1 mg/kg given to anesthetized chimpanzees results in complete inhibition of the pressure response to exogenous Ang II, with a plateau effect for 200 min followed by a steady decrease with a residual inhibitory effect of 50% as late as 24 hr (*19*). For confirmation of these published potencies, measurements were performed in three dogs. The pressure effects of multiple administrations of exogenous Ang II (0.1 mg/g intravenously) were completely abolished between 20 min and 2 hr after intravenous injection of 1 mg/kg MK-996. These measurements indicated that the

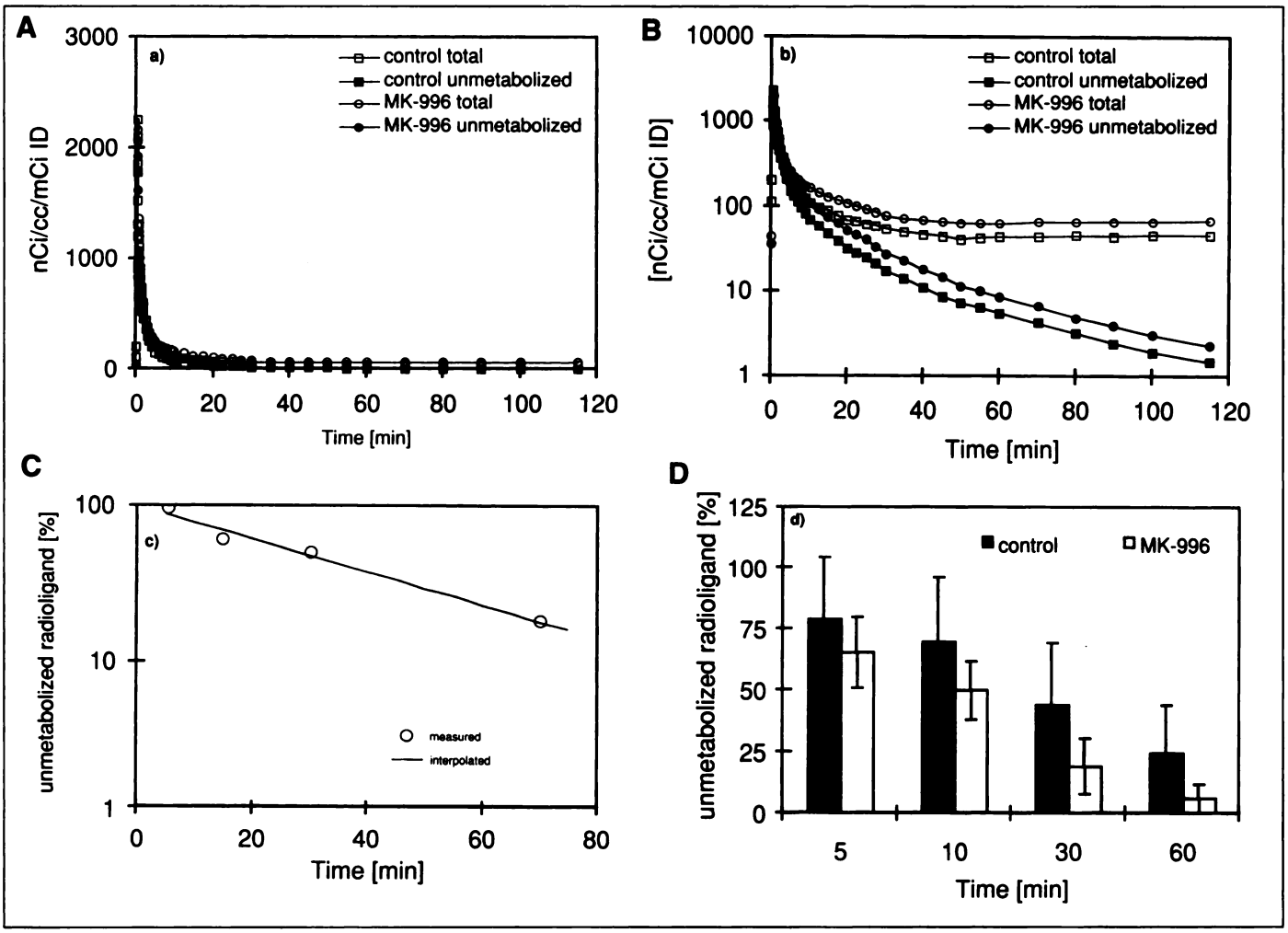

FIGURE 2. Input functions without and with metabolite correction. Using linear display (A), input function from post MK-996 is slightly higher than that obtained at control stage; this difference is more obvious on semilogarithmic graph (B). Percentage of unmetabolized radioligand in arterial plasma can be interpolated by simple monoexponential regression (C). This unmetabolized fraction decreases with time and is less during the MK-996 study than during control study (D). Values represent mean ± s.d. (n = 6).

given dose of 1 mg/kg is sufficient to achieve an equilibrium of receptor blockade throughout a typical PET study.

In all studies and at all times during image acquisition, radioactivity was higher in the renal cortex than in the medulla (Fig. 1). Autoradiographic studies show that in vivo AT_1-selective radioligands preferentially bind to receptors in the renal cortex. The opposite happens in vitro when preferential

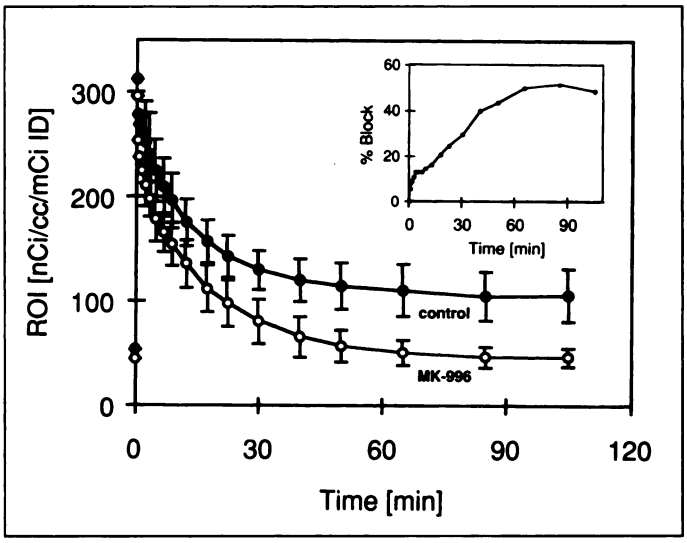

FIGURE 3. Renal cortical time-activity curves for control and MK-996 blocking study. Percentage difference between two studies increases with time and appears to plateau around 60 min postinjection (box inset). Values represent mean ± s.d. (n = 6).

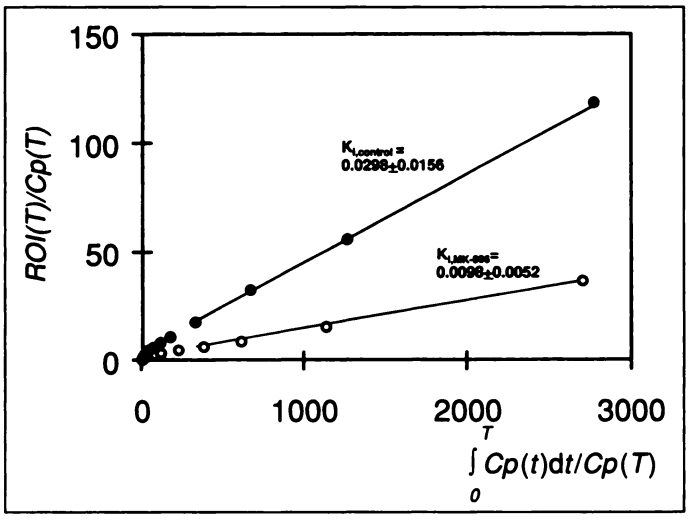

FIGURE 4. Average Gjedde-Patlak plot calculated from six control and MK-996 studies. A significant reduction of slope illustrates inhibition of radioligand binding due to blockade of AT_1 receptors by MK-996.

binding of these ligands to the renal medulla is observed (*20*). Possible explanations for this difference in binding are:

1. Lower blood flow to the medulla than to the cortex;
2. Occupancy of the medullary receptors in vivo by endogenous Ang II; or
3. Higher Ang II-mediated receptor internalization in the medulla.

Possible limitations of the radioligand include excretion through the kidneys and liver. Excretion through the kidneys was minimal during the experiments (Fig. 1); however, further investigation of pharmacologically active or inactive ^{11}C-labeled metabolites in the kidneys is warranted. Although the radioligand enters the bowel lumen by way of hepatobiliary excretion, an appropriate separation of these structures and the renal cortical regions of interest (under exclusion of gastrointestinal activity) is possible (Fig. 1C).

Consistent with the differences in the arterial time-activity curves, both total and unmetabolized radioactivity time integrals were lower for the control studies than for the blocking studies with MK-996. The time integral represents the availability of the radioligand throughout the entire course of the study. The differences between the arterial input functions clearly indicate that reduced binding of the radioligand after MK-996 was attributable not to reduced radioligand delivery but to reduced accumulation at specific binding sites.

Time-activity curves in the cortices of the kidneys demonstrated a prominent peak followed by fast and then slow washout. The early peak corresponds to first-pass distribution of the radioligand within the vasculature of the kidney. The following washout component is probably related to the distribution of the radioligand within a virtual compartment that corresponds to nonspecific binding sites, whereas the slowest component with an almost steady level of radioactivity and binding inhibition after 60 min is related to specific binding. Therefore, the images obtained at 60 min and later can be used for receptor imaging. Blocking effects of the AT_1 antagonist MK-996 were strongest during this later period. The relatively low binding inhibition of 50% seen in the time-activity curves is the result of a larger amount of radioligand available due to blockade of the receptors in the entire body. Inhibition is higher when parameter K is used for quantification, e.g., 66%. The Gjedde-Patlak plot is a simplified way of quantifying radioligand uptake and binding. This technique is applied for kinetic analysis of radioligands with a component of irreversible binding and largely eliminates the effect of the input function. Thus, if one excludes the effect of higher ligand availability after receptor blockade, at least two-thirds of renal cortical radioactivity is due to specific binding to the AT_1 receptors.

CONCLUSION

The presented data demonstrate that PET imaging of the renal cortical AT_1 receptors is feasible with ^{11}C-L-159,884. The quality of the images is good, and the time-activity curves illustrate the blocking effect of the AT_1 receptor antagonist MK-996 on radioligand binding. Based on the influx rate constant K, at least two-thirds of the radioactivity corresponds to specific binding, which makes this radioligand suitable for quantitative studies of the AT_1 receptors.

ACKNOWLEDGMENTS

We appreciate Robert Smoot, CNMT, for his assistance with the radiochemical synthesis and David Clough, CNMT, for organization and performance of the PET studies. We thank Paige Finley for her excellent help in the dog studies. This work was in part supported by NIH Grant No. DK50183.

REFERENCES

1. Bernstein KE, Alexander RW. Counterpoint: molecular analysis of the angiotensin II receptor. *Endocr Rev* 1992;13:381–386.
2. Griendling KK, Murphy TJ, Alexander RW. Molecular biology of the renin-angiotensin system. *Circulation* 1993;87:1816–1828.
3. Gibson RE, Thorpe HH, Cartwright ME, et al. Angiotensin II receptor subtypes in renal cortex of rats and rhesus monkeys. *Am J Physiol* 1991;261:F512–F518.
4. Wood AJJ. Angiotensin receptors and their antagonists. *N Engl J Med* 1996;334:1649–1654.
5. Ferrario CM. The renin-angiotensin system: importance in physiology and pathology. *J Cardiovasc Pharmacol* 1990;15(suppl 3):S1–S5.
6. Caulfield M, Lavender P, Farrall M, et al. Linkage of the angiotensinogen gene to essential hypertension. *N Engl J Med* 1994;330:1629–1633.
7. Admiraal PJ, Danser AH, Jong MS, Pieterman H, Derkx FH, Schalekamp MA. Regional angiotensin II production in essential hypertension and renal artery stenosis. *Hypertension* 1993;21:173–184.
8. Chang RSL, Bendesky RJ, Chen TS, et al. In vitro pharmacology of MK-996, a new potent and selective angiotensin II (AT_1) receptor antagonist. *Drug Dev Res* 1994;32:161–171.
9. Chakravarty PK, Naylor EM, Chen A, et al. A highly potent, orally active imidazo [4,5-b]pyridine biphenyl acylsulfonamide (MK-996;L-159,282): a new AT1-selective angiotensin II receptor antagonist. *J Med Chem* 1994;37:4068–4072.
10. Lappe JT, Toh J, Soffer BA, Goldberg AI, Sweet CS. Efficacy and tolerability of multiple doses of MK-996, an angiotensin II (AII) receptor antagonist, compared to enalapril and to placebo in mild to moderate hypertensive patients [Abstract]. *Am J Hypertens* 1995;8:180A.
11. Dannals RF, Ravert HT, Frost JJ, Wilson AA, Burns HD, Wagner HN Jr. Radiosynthesis of an opiate receptor binding radiotracer: [^{11}C]carfentanil. *Int J Appl Radiat Isot* 1985;36:303–306.
12. Hamill TG, Burns HD, Dannals RF, et al. Development of [^{11}C]L-159,884: a radiolabeled, nonpeptide angiotensin II antagonist that is useful for angiotensin II, AT_1 receptor imaging. *Appl Radiat Isot* 1996;47:211–218.
13. Gjedde A. Calculation of glucose phosphorylation from brain uptake of glucose analogs in vivo: a re-examination. *Brain Res* 1982;4:237–274.
14. Patlak CS, Blasberg RG, Fenstermacher JD. Graphical evaluation of blood-to-brain transfer constants from multiple-time uptake data. *J Cereb Blood Flow Metab* 1983;3:1–7.
15. Patlak CS, Blasberg RG. Graphical evaluation of blood-to-brain transfer constants from multiple-time uptake data. Generalizations. *J Cereb Blood Flow Metab* 1985;5:584–590.
16. Carson RE. Mathematical modeling and compartmental analysis. In: Harbert JC, Eckelman WC, Neumann RD, eds. *Nuclear medicine diagnosis and therapy*. New York: Thieme; 1996:167–193.
17. Kim SE, Scheffel U, Szabo Z, et al. In vivo labeling of angiotensin II receptors with a carbon-11 labeled selective nonpeptide antagonist. *J Nucl Med* 1996;37:307–311.
18. Burns L, Clark KL, Bradley J, Robertson MJ, Clark AJL. Molecular cloning of the canine angiotensin II receptor–an AT_1-like receptor with reduced affinity for DuP753. *FEBS Lett* 1994;343:146–150.
19. Kivlighn SD, Zingaro GJ, Gabel RA, et al. In vivo pharmacology of a novel AT_1 selective angiotensin II receptor antagonist, MK-996. *Am J Hypertens* 1995;8:58–66.
20. Zhuo J, Alcorn D, McCausland J, Casley D, Mendelsohn FAO. In vivo occupancy of angiotensin II subtype 1 receptors in rat renal medullary interstitial cells. *Hypertension* 1994;23:838–843.